A reduced-order observer based LQR control method for Roll-to-Roll systems

Zhanpeng He, Zhihua Chen, Xueqin Huang, Dong Ma

Institute of Computing Technology, Guangzhou University, China, Guangdong, Guangzhou, 510006
(Tel: +8613119536446; e-mail: 2112006102@e.gzhu.edu.cn; czhgd@gzhu.edu.cn; 2112006109@e.gzhu.edu.cn; 2112006033@e.gzhu.edu.cn).

Abstract: Roll-to-Roll (R2R) manufacturing is a flexible material manufacturing process with a high degree of automation and a low degree of cost. But the complex characteristics make the high-precision register control a critical challenge. In this paper, a reduced-order observer is designed to estimate the tension fluctuation value, and the estimated value is used to calculate the optimal control quantity through a linear quadratic regulator (LQR). Combined with the decoupling algorithm, a high-precision reduced-order observer based LQR control (LQRC) is achieved. Simulations and comparisons confirm that the register control method has improved the control accuracy and adjustment time. Compared with the published FDPD, the control accuracy of LQRC is improved by at least 47%, and the adjustment time is reduced by at least 55%. The LQRC method has smoother control signal and consumes less energy compared with the FDPD control method. The results indicate that LQRC method has good robustness and advantages in practical application of industry.

Keywords: Roll-to-Roll (R2R) printing systems; register control; reduced-order observer; LQR control (LQRC)

1. INTRODUCTION

The R2R manufacturing is widely used in the production of flexible materials because of its low manufacturing cost and high degree of automation (Jung et al., 2014; Palavesam et al., 2018; Lee et al., 2019). The typical application of the R2R manufacturing is the R2R printing machines (Figure 1 is a schematic diagram of the R2R printing system used in the industry), and the key criterion is the register error accuracy (Abbel et al., 2018). The tension fluctuation of the printing material (called web) leads to the register errors, and the tension fluctuation is caused by many factors such as disturbances and velocity changes. The R2R system is a complex coupling system with multi-inputs and multi-outputs. A high-precision register control is extremely important for R2R printing systems, but the control law is not trivial because of the complex coupling (Lee et al., 2020; Lee et al., 2020).

Figure 1. A R2R printing system used in the industry.

Some literatures have been studied on the register control of R2R systems. (Yoshida et al., 2008; Yoshida, 2008) deduced the register errors model and proposed a feedforward PD control method to eliminate the influence of the upstream control quantities on the downstream printing units, which improved the register accuracy of the R2R printing systems. Using new governing equations to minimize the effect of web tension on downstream printing units, (Torres and Pagilla, 2018) reduced the propagation of lateral perturbations. (Zhou et al., 2016) designed a control method for R2R systems for micro-contact printing to completely eliminate the coupling effect of the lateral motion of the web, and achieved a precise control of ±200 nm. (Nguyen et al., 2018) proposed a hyperbolic partial differential equation control method with two control inputs to reduce the lateral vibration of the web. An intelligent nonlinear tension and speed controller was designed by (Kim et al., 2020) to improve the disturbance rejection performance and offset-free property for R2R printing systems. (Zhang et al., 2020) proposed a direct-decoupling PD control method, which completely eliminated the register errors caused by upstream control quantities. A fully decoupled PD control algorithm was proposed to completely eliminate the complex coupling relationship by (Chen et al., 2020), and therefore improve the register accuracy.

The application of R2R systems in high-tech products put forward higher requirements for register accuracy such as solar thin-film cells and flexible circuit boards (Dou et al., 2018; Gao et al., 2016; Bariya et al., 2018; Wang et al., 2021). Optimal controls have rich theoretical support (Kim et al., 2010; Neilan et al., 2010) and been widely used in various industries (Buchholz et al., 2013; Zulkowski and DeWeese, 2015). In this paper, a reduced-order observer based LQR optimal control method have been proposed to estimate the tension fluctuation value. According to the estimated tension fluctuation and measured register errors, a linear quadratic regulator (LQR) is designed to calculate the optimal feedback control quantities. Experiments and comparisons proved that the accuracy and adjustment time of the LQR control method proposed in the paper have been improved obviously.

The following is the structure of this paper. In section 2, a reduced-order observer is designed based on the mathematical model of R2R printing systems to estimate the tension fluctuation. In section 3, a linear quadratic optimal control is designed based on the estimated state variables. In section 4, simulation and comparisons are carried out by Matlab and Simulink to verify the effectiveness of the proposed LQR control algorithm. The conclusion is given in section 5.

2. DESIGN OF REDUCED-ORDER OBSERVER

Please use this document as a template to prepare your manuscript. For submission guidelines, follow instructions on the paper submission system as well as the conference website.

The simplified diagram of two adjacent printing units is shown in Figure 2. Each printing unit will print a mark and this mark will run to the next printing unit as the reference. Then the register error will be detected by a high-precision photoelectric device (sensor), which is the misaligned distance of two adjacent marks. The technological nomenclature used in this paper are listed in Table 1.

Table 1. Nomenclature

r	Radius of gravure cylinder
K	Elasticity coefficient
ω^*	Angular velocity of gravure cylinder at steady state
T^*	Web tension at steady state
l_i	Web length between *No.i* and *No. (i + 1)* gravure cylinder
$T_i(t)$	Web tension between *No. i* and *No. (i + 1)* gravure cylinder at time *t*
$\omega_i(t)$	Angular velocity of *No. i* gravure cylinder at time *t*
$E_i(t)$	Register errors between *No. (i + 1)* and No.i unit at time t
$\Delta T_i(t)$	Tension fluctuation between *No. i* and *No. (i + 1)* gravure cylinder at time t
$\Delta\omega_i(t)$	Variation of angular velocity of *No. i* gravure cylinder at time t

In Figure 2, T_i is the web tension which is the sum of ΔT_i and T^*; ω_i is the angular velocity which sum of the $\Delta\omega_i$ and ω^*. According to the law of conservation of mass, the relationship among the angular velocity of the gravure cylinder, the tension of web and the register errors, that is, the differential equation

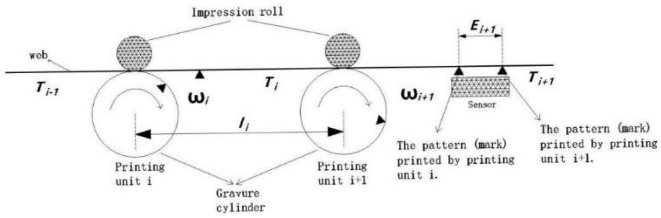

Figure 2. The simplified diagram of the adjacent unit of R2R printing systems.

model of the R2R printing systems is as follows (Chen et al., 2020):

$$\begin{cases} \dfrac{d\,\Delta T_i(t)}{dt} = \dfrac{\omega^* r}{l_i}\big(\Delta T_{i-1}(t) - \Delta T_i(t)\big) + \\ \qquad\qquad \dfrac{(1+KT^*)r}{Kl_i}\big(\Delta\omega_{i+1}(t) - \Delta\omega_i(t)\big) \\ \dfrac{d\,\Delta T_i(t)}{dt} = \dfrac{K\omega^* r}{1+KT^*}\Delta T_i(t) \end{cases} \tag{1}$$

Define $a_i = \omega^* r / l_i$, $b_i = (1+KT^*)r/Kl_i$, $c = K\omega^* r/(1+KT^*)$.

For R2R printing systems, the control variable is the change of the angular velocity of gravure cylinder. To reduce the register errors caused by the tension fluctuation, a state observer is designed to estimate the tension fluctuation value. Make i=1 in (1), because the first mark printed by the first gravure cylinder is used as a reference, there are $\Delta\omega_1(t) = 0$ and $\Delta T_0(t) = 0$. Make *i=1*, *i=2*, $\cdots\cdots$, *i=i-1*, so we have $x(t) = [\Delta T_1(t), \Delta T_2(t), \cdots\cdots, \Delta T_{i-1}(t), \Delta E_2(t), \Delta E_3(t), \cdots\cdots, \Delta E_i(t)]^T$, $u(t) = [\Delta\omega_2(t), \Delta\omega_3(t), \cdots\cdots, \Delta\omega_i(t)]^T$ and $y(t) = [E_2(t), E_3(t), \cdots\cdots, E(t)]^T$, the continuous state space model of R2R printing systems can be obtained as follows:

$$\begin{cases} \dot{x(t)} = Ax(t) + Bu(t) \\ y(t) = C(t) \end{cases} \tag{2}$$

where $A = \begin{bmatrix} A_{11} & A_{12} \\ A_{21} & A_{22} \end{bmatrix}$, because *No.1* printing unit is the reference unit and it does not participate in the calculation of tension and error, matrix A_{11}、A_{12}、A_{21}、A_{22} both are *(i-1)* order square matrices:

$$A_{11} = \begin{bmatrix} -a_1 & 0 & 0 & \cdots & 0 & 0 \\ a_2 & -a_2 & 0 & \cdots & 0 & 0 \\ 0 & a_3 & -a_3 & \cdots & 0 & 0 \\ \vdots & \vdots & \vdots & \ddots & \vdots & \vdots \\ 0 & 0 & 0 & \cdots & -a_{i-2} & 0 \\ 0 & 0 & 0 & \cdots & a_{i-1} & -a_{i-1} \end{bmatrix} \tag{3}$$

$A_{21} = cI(i-1), A_{21} = A_{21} = O(i-1)$

where $B = [B_{11} \quad B_{21}]^T$, matrix B_{11}、B_{21} both are *(i-1)* order square matrices:

$$B_{11}=\begin{bmatrix} b_1 & 0 & 0 & \cdots & 0 & 0 \\ -b_2 & b_2 & 0 & \cdots & 0 & 0 \\ 0 & -b_3 & b_3 & \cdots & 0 & 0 \\ \vdots & \vdots & \vdots & \ddots & \vdots & \vdots \\ 0 & 0 & 0 & \cdots & b_{i-2} & 0 \\ 0 & 0 & 0 & \cdots & -b_{i-1} & b_{i-1} \end{bmatrix}, \tag{4}$$
$$B_{21}=O(i-1)$$

where $C=[C_{11} \quad C_{21}]$, matrix C_{11}、C_{21} both are *(i-1)* order square matrices:

$$C_{11}=O(i-1), C_{21}=I(i-1) \tag{5}$$

It is known that the observable PBH rank criterion: when the inputs of R2R printing systems satisfy $u(t)=0$, the sufficient and necessary condition for $[\Delta T_1(t), \Delta T_2(t), \cdots\cdots, \Delta T_{i-1}(t), \Delta E_2(t), \Delta E_3(t), \cdots\cdots, \Delta E_i(t)]^T$ to be completely observable is that the matrix $[sI-A \quad C]^T$ is full rank. That is, rank $[sI-A \quad C]^T=2(i-1)$, where *s* is the eigenvalue of the state matrix *A*, the *(i-1)* eigenvalues of the matrix *A* both are zero, and the other *(i-1)* eigenvalues both are *-a* (*a≠0*). It can be obtained that rank $[sI-A \quad C]^T=2(i-1)$ meets the observable criterion, so R2R printing systems have complete observability.

The output vectors are $[E_2(t), E_3(t), \cdots\cdots, E(t)]^T$, which are the last *(i-1)* state of the state vectors $x(t)$. Then the *(i-1)* state vectors of R2R printing systems can be directly replaced by the *(i-1)* output vectors. It is necessary to establish a *(i-1)* dimensionality reduced-order observer to reconstruct the remaining *(i-1)* state vectors.

Divide state vectors $x(t)=[\Delta T_1(t), \Delta T_2(t), \cdots\cdots, \Delta T_{i-1}(t), \Delta E_2(t), \Delta E_3(t), \cdots\cdots, \Delta E_i(t)]^T$ into $x_a(t)=[\Delta T_1(t), \Delta T_2(t), \cdots\cdots, \Delta T_{i-1}(t)]^T$ and $x_b(t)=[\Delta E_2(t), \Delta E_3(t), \cdots\cdots, \Delta E_i(t)]^T$. The (2) can be rewritten as follows:

$$\begin{cases} \begin{bmatrix} \dot{x_a}(t) \\ \dot{x_b}(t) \end{bmatrix} = \begin{bmatrix} A_{11} & A_{12} \\ A_{21} & A_{22} \end{bmatrix} \begin{bmatrix} x_a(t) \\ x_b(t) \end{bmatrix} + \begin{bmatrix} B_{11} \\ B_{21} \end{bmatrix} u(t) \\ y(t)=[C_{11} \quad C_{21}] \begin{bmatrix} x_a(t) \\ x_b(t) \end{bmatrix} = x_b(t) \end{cases} \tag{6}$$

Expand (6) we have:

$$\begin{cases} \dot{x_a}(t)=A_{11}x_a(t)+A_{12}y(t)+B_{11}u(t) \\ \dot{y}(t)=A_{21}x_a(t)+A_{22}y(t)+B_{21}u(t) \end{cases} \tag{7}$$

Let $z(t)=\dot{y}(t)-A_{22}y(t)-B_{21}u(t)$, the subsystem to be observed is:

$$\begin{cases} \dot{x_a}(t)=A_{11}x_a(t)+A_{12}y(t)+B_{11}u(t) \\ z(t)=A_{21}x_a(t) \end{cases} \tag{8}$$

$u(t)$ and $y(t)$ are known in (5), so $A_{12}y(t)+B_{11}u(t)$ can be used as an input in the subsystem, and $z(t)=\dot{y}(t)-A_{22}y(t)-B_{21}u(t)$ can be used as a known output in the subsystem; A_{11} is the state matrix of the subsystem, and A_{21} is the output matrix of the subsystem. According to the reduced-order observer design equation, we can get:

$$\begin{cases} \dot{w}=(A_{11}-GA_{21})w+(B_{11}-GB_{21})u \\ \quad +[(A_{11}-GA_{21})G+A_{12}-GA_{22}]y \\ \quad =(A_{11}-GA_{21})(w+Gy)+B_{11}u \\ \hat{x}_a=w+Gy \end{cases} \tag{9}$$

where *G* is *(i-1)×(i-1)* feedback matrix of the reduced-order observer, and the eigenvalues of the subsystem matrix $(A_{11}-GA_{21})$ can be arbitrarily configured through the pole configuration; w is the intermediate variables to obtain the reconstructed state vector $\hat{x}_a(t)$. Combined with $x_b(t)=y(t)$, the estimate of the entire state vectors $\hat{x}(t)$ can be expressed as follows:

$$\hat{x}(t)=\begin{bmatrix} \hat{x}_a(t) \\ x_b(t) \end{bmatrix} = \begin{bmatrix} w+Gy \\ y(t) \end{bmatrix} \tag{10}$$

According to (9) and (10), the structure diagram of the reduced-order observer is shown in Figure 3.

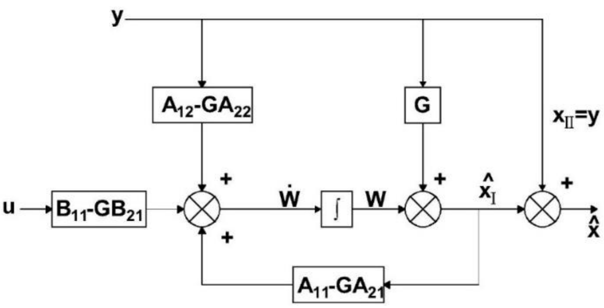

Figure 3. The structure diagram of reduced-order observer.

Since the whole output vectors of the system can directly replace half of the state vectors, the error $e_a(t)$ between the real state vectors and the estimated state vectors of the remaining part is defined as:

$$e_a(t)=x_a(t)-\hat{x}_a(t) \tag{11}$$

Then take the derivation of (11) and according to (7), (9) and (10), we can get

$$\begin{aligned} \dot{e_a}(t) &= \dot{x_a}(t)-\dot{\hat{x}}_a(t) \\ &= A_{11}x_a(t)+A_{12}y(t)+B_{11}u(t)-\dot{w}(t)-G\dot{y}(t) \\ &= A_{11}x_a(t)+A_{12}y(t)+B_{11}u(t)\dot{w}(t) \\ &\quad -[(A_{11}-GA_{21})(w+Gy)+B_{11}u] \\ &\quad -G[A_{21}x_a(t)+A_{22}y(t)+B_{21}u(t)] \\ &= A_{11}x_a(t)-(A_{11}-GA_{21})\hat{x}_a(t)-GA_{21}x_a(t) \\ &= (A_{11}-GA_{21})e_a(t) \end{aligned} \tag{12}$$

It can be seen from (12) that $e_a(t)$ can converge to 0 as long as the matrix $(A_{11}-GA_{21})$ is configured as a negative diagonal matrix, that is, the reduced-order observer gain matrix *G* should be configured at a suitable position through the pole configuration. In this paper, the main considerations are the rapid convergence of the tension estimation and the good poles. The poles configuration of the reduced-order observer in this paper is based on engineering practice.

3. CONTROL METHOD

3.1 LQR control

The state space equation and state feedback control law of No.i printing unit is:

$$\dot{x}_i(t) = A_i x_i(t) + B_i \Delta\omega_i(t) \tag{13}$$

$$\Delta\omega_i(t) = -K_i \hat{x}_i(t) = -K_{i1}\widehat{\Delta T}_{i-1}(t) - K_{i2}E_i(t) \tag{14}$$

where $\hat{x}_i(t) = \begin{bmatrix} \widehat{\Delta T}_{i-1}(t) \\ E_i(t) \end{bmatrix}$, $A_i = \begin{bmatrix} -a_i & 0 \\ c & 0 \end{bmatrix}$, $B_i = \begin{bmatrix} b_i \\ 0 \end{bmatrix}$, and $K_i = [K_{i1} \quad K_{i2}]$ is the state feedback gain matrix for *No.i* printing unit.

The value of the state feedback gain matrix can be solved by configuring the poles, but it is difficult to select the appropriate poles, and it is impossible to guarantee that the poles can achieve optimal control. Therefore, the state feedback control method in this paper adopts the Linear Quadratic Regulator (LQR) to obtain the optimal control. It is necessary to set a performance function. The performance function of No.i printing unit is defined as:

$$\begin{aligned} J_i = &\frac{1}{2} x_i^T(t_{start}) L_i x_i(t_{start}) \\ &+ \frac{1}{2}\int_{t_{start}}^{t_{end}} [\hat{x}_i^T(t) Q_i \hat{x}_i(t) + \Delta\omega_i^T(t) R_i \Delta\omega_i(t)] dt \end{aligned} \tag{15}$$

where L_i is a semi-positive definite terminal weighting matrix, Q_i is a semi-positive definite state weighting matrix, and R_i is a positive definite control weighting matrix. According to the minimum value principle, a 2-dimensional Lagrange multiplier vector $\lambda_i(t)$ is introduced to construct a Hamiltonian function to obtain the optimal control variable $\Delta\omega_i^*(t)$:

$$\begin{aligned} H_i[x,u,\lambda,t] = &\frac{1}{2}[\hat{x}_i^T(t) Q_i \hat{x}_i(t) + \Delta\omega_i^T(t) R_i \Delta\omega_i(t)] \\ &+ \lambda_i^T [A_i x_i(t) + B_i \Delta\omega_i(t)\ ] \end{aligned} \tag{16}$$

H_i should also obtain an extreme value under the optimal control. According to the method of finding the extreme value of the multivariate function, the partial derivative function of $\Delta\omega_i(t)$ is obtained by (16):

$$\frac{\partial H_i}{\partial \Delta\omega_i(t)} = R_i \Delta\omega_i(t) + B_i^T \lambda_i(t) \tag{17}$$

Make $(17) = 0$, since the matrix $R_i(t)$ is positive definite and symmetric, we have:

$$\Delta\omega_i^*(t) = -R_i^{-1} B_i^T \lambda_i(t) \tag{18}$$

And $\partial^2 H_i / \partial[\Delta\omega_i(t)]^2 = R_i$, R_i is positive definite, so (18) is the desired optimal control which make performance function J_i reach a minimum value.

In the same way, the partial derivatives of $\lambda_i(t)$ and $x_i(t)$ can be calculated by (17):

$$\begin{cases} \dot{\lambda_i}(t) = \dfrac{\partial H_i}{\partial x_i} = -Q_i \hat{x}_i(t) - A_i^T \lambda_i(t) \\ \dot{\hat{x}_i}(t) = \dfrac{\partial H_i}{\partial \lambda_i} = A_i \hat{x}_i(t) + B_i \Delta\omega_i(t) \\ \qquad = A_i \hat{x}_i(t) - B_i R_i^{-1} B_i^T \lambda_i(t) \end{cases} \tag{19}$$

The initial and equilibrium conditions are:

$$\begin{cases} x_i(t_{start}) = x_0 \\ \lambda_i(t_{end}) = \dfrac{\partial}{\partial x_i(t_{end})}\left[\dfrac{1}{2} x_i^T(t_{end}) L_i x_i(t_{end})\right] \\ \qquad = L_i x_i(t_{end}) \end{cases} \tag{20}$$

Equation (20) can be solved according to the initial and equilibrium conditions (17).

We know that $\Delta\omega_i^*(t)$ is a linear function of $\lambda_i(t)$ from (15). The transformation matrix P_i is a 2×2-dimensional real symmetric positive definite matrix, then:

$$\lambda_i(t) = P_i(t) \hat{x}_i(t) \tag{21}$$

Substitute (21) into (18):

$$\begin{cases} \Delta\omega_i^*(t) = -K_i \hat{x}_i(t) = -R_i^{-1} B_i^T P_i(t) \hat{x}_i(t) \\ K_i = R_i^{-1} B_i^T P_i(t) = [K_{i1} \quad K_{i2}] \end{cases} \tag{22}$$

According to (18), the differential equation of the closed-loop system of *No.i* printing unit is:

$$\begin{aligned} \dot{\hat{x}_i}(t) = [&A_i \\ &- B_i R_i^{-1} B_i^T P_i(t) \hat{x}_i(t)] \hat{x}_i(t) \end{aligned} \tag{23}$$

Equation (23) shows that the optimal control can be realized by the optimal linear feedback composed of state vectors, then the optimal control quantity of the state feedback is calculated below.

Substituting (21) into (19) and eliminating $\lambda_i(t)$, we can get:

$$\begin{cases} \dot{\lambda_i}(t) = -Q_i(t) \hat{x}_i(t) - A_i^T P_i(t) \hat{x}_i(t) \\ \dot{\hat{x}_i}(t) = A_i \hat{x}_i(t) - B_i R_i^{-1} B_i^T P_i(t) \hat{x}_i(t) \end{cases} \tag{24}$$

At the same time, derivation of equation (18) is as follows:

$$\dot{\lambda_i}(t) = \dot{P_i}(t) \hat{x}_i(t) + P_i(t) \dot{\hat{x}_i}(t) \tag{25}$$

Substitute (24) into (25), we get:

$$\begin{aligned} &-Q_i(t) \hat{x}_i(t) - A_i^T P_i(t) \hat{x}_i(t) \\ &= \dot{P_i}(t) \hat{x}_i(t) + P_i(t)[A_i \hat{x}_i(t) - B_i R_i^{-1} B_i^T P_i(t) \hat{x}_i(t)] \end{aligned} \tag{26}$$

After arranging (26), the result is as follows:

$$\begin{aligned} &\dot{P_i}(t) = \\ &-Q_i(t) - A_i^T P_i(t) - P_i(t) A_i + P_i(t) B_i R_i^{-1} B_i^T P_i(t) \end{aligned} \tag{27}$$

The value of the transformation matrix $P_i(t)$ can be obtained combined with the condition $P_i(t_{end}) = L_i$. Finally, substituting $P_i(t)$ back into the (19), the optimal control amount $\Delta\omega_i^*(t)$ of *No. i* printing unit can be calculated.

3.2 Decoupling

Because the upstream control quantities will cause the downstream register errors, it is necessary to eliminate the downstream register errors caused by the upstream control quantities. The decoupling compensation based on the model of (1) is as follows (Chen et al., 2020):

$$\begin{cases} \Delta\omega_{ij}^{RC}(s) = F_j(s)\Delta\omega_j^*(s) \\ F_j(s) = \dfrac{s}{s + a_{j-1}} \end{cases} \tag{28}$$

where a_{j-1} is the system parameter, $a_{j-1} = \omega^* r / l_{j-1}$; $\Delta\omega_j^*(s)$ is the optimal control quantity required by the *No. j* printing unit to eliminate the measured register errors; $\Delta\omega_{ij}^{RC}(s)$is the decoupling control amount for the *No. i* printing unit to eliminate the register errors caused by the register control amount of *No. j* printing unit.

Now, the sum of the control amount for each printing unit is:

$$u^*(t) = \Delta\omega_i^*(t) + \sum_{j=2}^{i-1} \Delta\omega_{ij}^{RC}(t)$$
$$= \begin{bmatrix} 1 & 0 & 0 & \cdots & 0 & 0 \\ F_2(t) & 1 & 0 & \cdots & 0 & 0 \\ F_2(t) & F_3(t) & 1 & \cdots & 0 & 0 \\ \vdots & \vdots & \vdots & \ddots & \vdots & \vdots \\ F_2(t) & F_3(t) & F_4(t) & \cdots & 1 & 0 \\ F_2(t) & F_3(t) & F_4(t) & \cdots & F_{i-1}(t) & 1 \end{bmatrix} \begin{bmatrix} \Delta\omega_2^*(t) \\ \Delta\omega_3^*(t) \\ \Delta\omega_4^*(t) \\ \vdots \\ \Delta\omega_{i-1}^*(t) \\ \Delta\omega_i^*(t) \end{bmatrix} \tag{29}$$

Combining 3.1 LQR control and 3.2 decoupling control, the structure diagram of the control method proposed in this paper is shown in Figure 4.

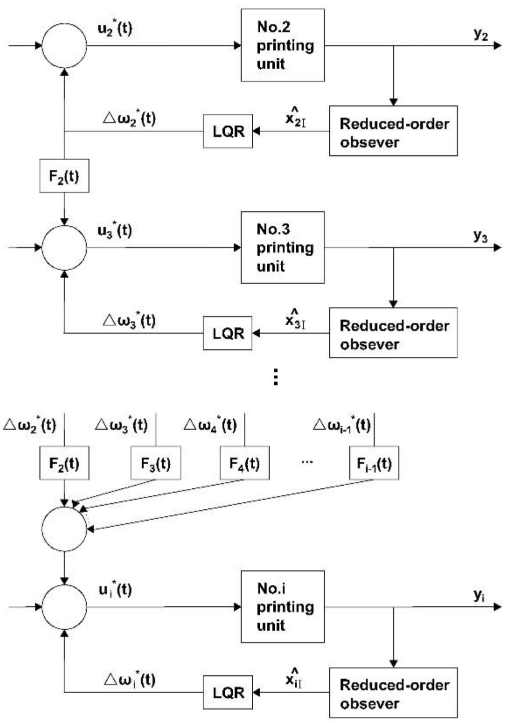

Figure 4. Structure of proposed control method.

Therefore, the state space model of R2R printing systems after decoupling can be written as:

$$\begin{cases} \dot{x}(t) = \begin{bmatrix} A_1^{RC} & A_2^{RC} \\ A_3^{RC} & A_4^{RC} \end{bmatrix} x(t) + \begin{bmatrix} B_1^{RC} \\ B_2^{RC} \end{bmatrix} u(t) \\ y(t) = \begin{bmatrix} C_{11} & C_{12} \end{bmatrix} x(t) \end{cases} \tag{30}$$

where A_1^{RC}, A_2^{RC}, A_3^{RC}, A_4^{RC}, B_1^{RC}, B_2^{RC} both are *(i-1)* order square matrices:

$$A_1^{RC} = \begin{bmatrix} -a_1 & 0 & 0 & \cdots & 0 & 0 \\ 0 & -a_2 & 0 & \cdots & 0 & 0 \\ 0 & 0 & -a_3 & \cdots & 0 & 0 \\ \vdots & \vdots & \vdots & \ddots & \vdots & \vdots \\ 0 & 0 & 0 & \cdots & -a_{i-2} & 0 \\ 0 & 0 & 0 & \cdots & 0 & -a_{i-1} \end{bmatrix}$$
$$A_2^{RC} = cI(i-1), A_3^{RC} = A_4^{RC} = O(i-1),$$
$$B_1^{RC} = \begin{bmatrix} b_1 & 0 & 0 & \cdots & 0 & 0 \\ 0 & b_2 & 0 & \cdots & 0 & 0 \\ 0 & 0 & b_3 & \cdots & 0 & 0 \\ \vdots & \vdots & \vdots & \ddots & \vdots & \vdots \\ 0 & 0 & 0 & \cdots & b_{i-2} & 0 \\ 0 & 0 & 0 & \cdots & 0 & b_{i-1} \end{bmatrix}, B_2^{RC} = 0, \tag{31}$$
$$u(t) = \begin{bmatrix} \Delta\omega_2^*(t) \\ \Delta\omega_3^*(t) \\ \Delta\omega_4^*(t) \\ \vdots \\ \Delta\omega_{i-1}^*(t) \\ \Delta\omega_i^*(t) \end{bmatrix}$$

It is easy to see that (30) is a simple non-coupled MIMO system, where $\Delta\omega_i^*(t) = -R_i^{-1}B_i^T P_i(t)\hat{x}_i(t)$ is the LQR control quantity designed based on the reduced-order tension observer.

4. INDUSTRIAL APPLICATION

Model (1) has been validated in (Chen et al., 2020), so it can be considered as a real situation of R2R printing systems. In this paper, a seven printing units electronic shaft gravure printing machine is used as an example to verify the effectiveness and superiority of the LQRC algorithm. The system parameters are shown in Table 2, and the poles of the designed reduced-order tension observer are shown in Table 3. The feedback matrix G of the reduced-order observer calculated from the configured poles is:

$$G = \begin{bmatrix} 4399.2 & 0 & 0 & 0 & 0 & 0 \\ 702.18 & 4026.4 & 0 & 0 & 0 & 0 \\ 0 & 702.18 & 3932.2 & 0 & 0 & 0 \\ 0 & \vdots & 702.18 & 1269.8 & 0 & 0 \\ 0 & 0 & 0 & 702.18 & 1095.9 & 0 \\ 0 & 0 & 0 & 0 & 702.18 & 1682 \end{bmatrix}$$

4.1 The closed-loop control

Given an initial disturbance with 3mm to No.2 printing unit, the register errors of No.2 printing unit to No.7 printing unit are shown in Figure 5. It can be seen from Figure 5(a) that the register errors can be reduced to 0.1mm after 42 sampling cycles and be kept within ±0.01mm after 55 sampling cycles. The adjustment time is only 55 sampling cycles, and there is no excessive overshoot. Similarly, it can be seen from Figure 5(b) that the decoupling algorithm eliminates the register errors of downstream printing units caused by the control quantities of upstream printing units. And the register errors of No.3 printing unit to No.7 printing unit can be kept within ±0.006mm. This closed-loop register control of No.2 printing unit to No.7 printing unit proves the effectiveness of LQRC method.

Table 2. System parameters

Parameters	Values
Printing speed	100(m/min)
Web length l_i	6.48(m)
Circumference of gravure cylinder r	0.53(m)
Web tension at steady state T^*	100(N)
Elasticity coefficient K	2.3×10^{-4}(1/N)

Table 3. The poles of reduced-order observer

Unit	Pole
No.2 printing unit	-1.8686
No.3 printing unit	-1.7320
No.4 printing unit	-1.6975
No.5 printing unit	-0.7223
No.6 printing unit	-0.6586
No.7 printing unit	-0.8732

4.2 Comparisons and Analysis

The comparisons of the LQR control algorithm (LQRC) and the fully decoupled PD control algorithm (FDPD) [14] are shown in Figure 6. It can be seen from Figure 6(a) that the adjustment time of No.2 printing unit of the LQRC algorithm and the FDPD algorithm is similar, but the LQRC algorithm has a smaller overshoot than the FDPD algorithm. As for the performance of the two algorithms in No.3 printing unit to No.5 printing unit in Figure 6(b), the LQRC algorithm has a 2-5 times improvement in register errors compared with the FDPD algorithm. In terms of adjustment time, the adjustment time of the LQRC algorithm is only 50% that of the FDPD algorithm. It can be seen from Figure 6(c) that the adjustment time of the LQRC algorithm on No.6 printing unit and No.7 printing unit is only 30% that of the FDPD algorithm.

It is known that the violent change of control signal will lead to a huge impact on the motor, serious bearing wear and energy waste. The absolute values of each printing unit control amount of the LQRC and FDPD are summed up respectively, and the results are shown in Figure 7. The sum of the absolute values of each printing unit control amount of the FDPD method is kept at about 21mm, while the LQRC method can be kept below 13mm. The results show that the LQRC method is more stable and smoother than that of FDPD method, which is more economical and applicable.

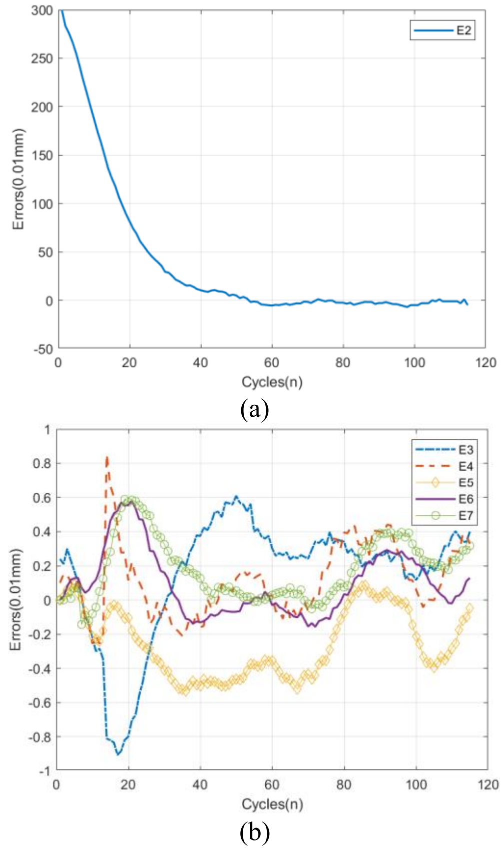

Figure 5. Closed-loop register control errors of No.2 printing unit to No.7 printing unit.

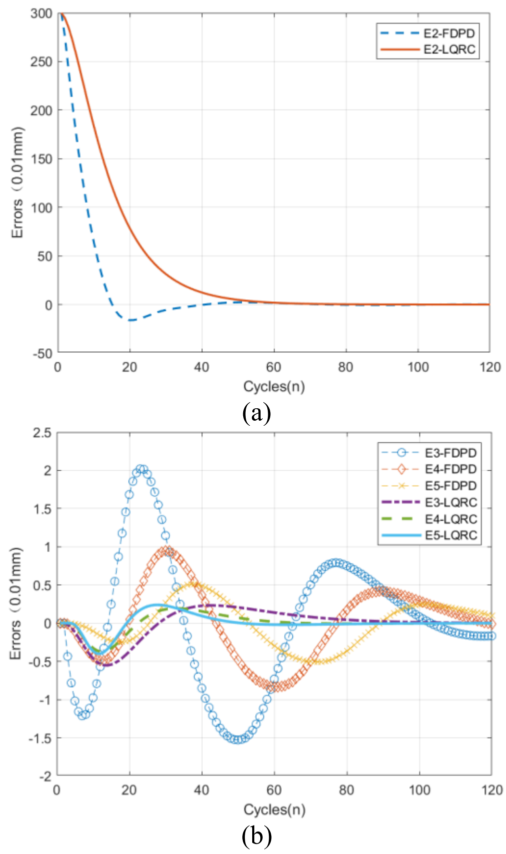

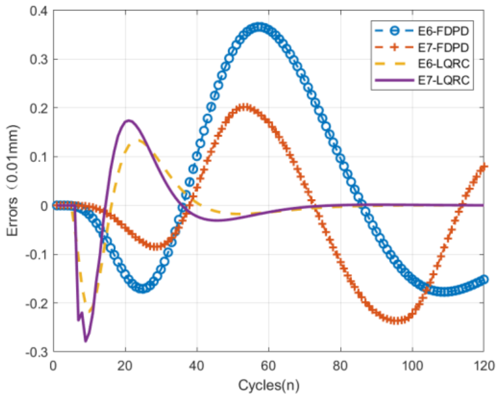

(c)

Figure 6. Comparison of register error between LQRC and FDPD.

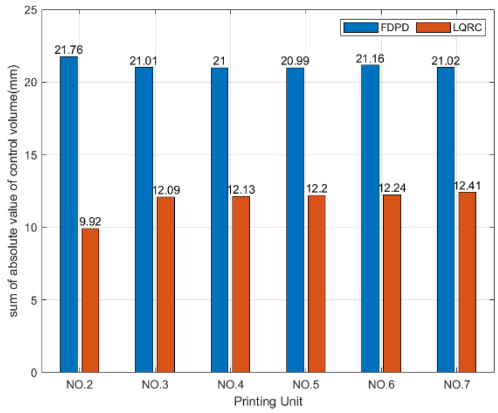

Figure 7. Comparison of the sum of absolute value of the control value of each printing unit of FDPD and LQRC (mm).

4.3 Anti-noise performance analysis

In order to analyze the anti-noise ability of LQRC, the bounded white noise module is used as the noise inputs to No.2 printing unit to No.4 printing unit. Figure 8 shows the comparisons of the register errors of No.2 printing unit to No.4 printing unit with and without noise. It is obvious from Figure 8(a) that the register errors of No.2 printing unit also drop rapidly to the range of ±0.01mm in the presence of noise, and the control curve is close to the curve without noise. It is obvious from Figure 8(b) that the register errors of No.3 printing unit and No.4 printing unit can be controlled within ±0.006mm with or without noise, and the control performances have certain similarity. The results indicate that LQRC method is robust to bounded noise disturbances.

4.4 Parameter sensitivity analysis

The web length in equation (1) is a key system parameter and obtained by manual measurement. So there is inevitably a certain range of measurement noise. Therefore, it is necessary to verify the sensitivity of LQRC algorithm to the key parameter. In this simulation, the web length of No.5 printing unit and No.6 printing unit are both 6.48m. The web length of No.5 printing unit is changed within the range of 86%-118%, and the web length of No.6 printing unit is changed within the range of 93%-126%. The register errors results calculated by using the LQRC algorithm are shown in Figure 9. It can be seen from Figure 9 that although the web length is not very accurate, the register errors of No.5 printing unit can be controlled within ±0.005mm, and the register errors of No.6 printing unit can be controlled within ±0.0025mm. Even if the web length has measurement errors, it does not affect the control effect of the LQRC, which shows that the LQRC has good fault tolerance and robustness to the measurement error of the web length.

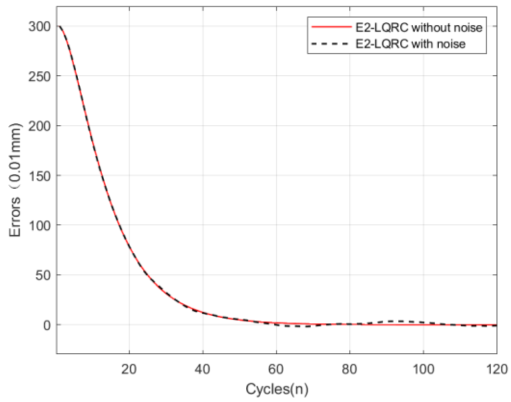

(a)

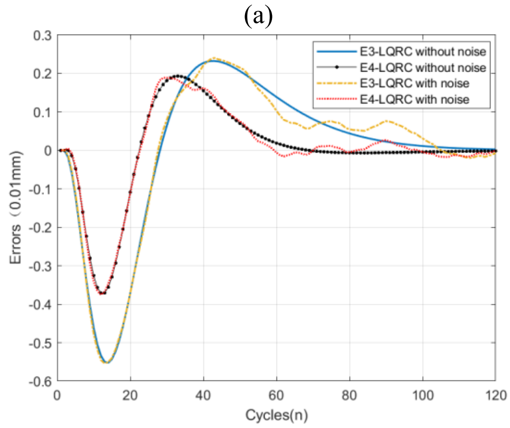

(b)

Figure 8. Comparisons of register errors from No.2 printing unit to No.4 printing unit with and without noise.

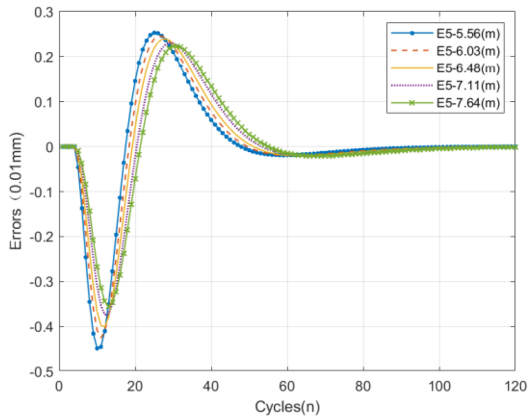

(a)

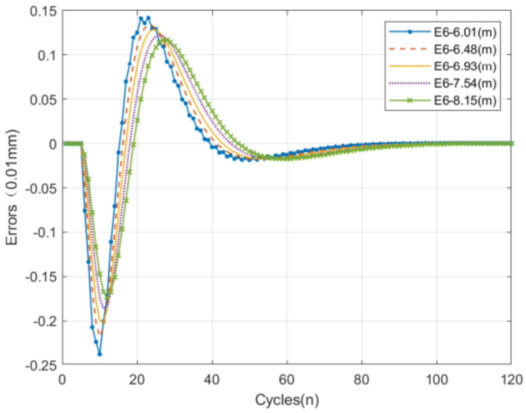

(b)

Figure 9. Comparison of register error to No.5 printing unit and No.6 printing unit under inaccurate web length l_i.

5. CONCLUSIONS

In this paper, a reduced-order observer based LQR control is proposed. Compared with the newly published FDPD method, the LQRC method has the rapidity of the adjustment time, the stability of control process, and the relative smoothness of control quantities. And the control accuracy improves at least 50% compared with the FDPD algorithm. At the same time, the sum of the absolute value of each printing unit control quantity is less than 60% that of the FDPD, which means that it not only impacts less wear and tear on the mechanical systems, but also saves large energy for productive process. Experiments and comparison experiments verified the control accuracy performance, anti-noise performance and parameter sensitivity. The above analysis results show that the LQRC method has good robustness and has great advantages in practical application of industry.

ACKNOWLEDGEMENTS

This work was supported by the Chinese National Natural Science Foundation under Grant 61876047.

REFERENCES

Abbel, R., Galagan, Y., & Groen, P. (2018). Roll‐to‐Roll Fabrication of Solution Processed Electronics. Advanced Engineering Materials, 20(8), 1701190.

Bariya, M., Shahpar, Z., Park, H., Sun, J., Jung, Y., Gao, W., ... & Javey, A. (2018). Roll-to-roll gravure printed electrochemical sensors for wearable and medical devices. *ACS nano, 12(7)*, 6978-6987.

Boscain, U., & Piccoli, B. (2005). An introduction to optimal control. *Contrôle non linéaire et applications,* Herman, Paris, 19-66.

Chen, Z., Zhang, T., Zheng, Y., Wong, D. S. H., & Deng, Z. (2020). Fully Decoupled Control of the Machine Directional Register in Roll-to-Roll Printing System. *IEEE Transactions on Industrial Electronics, 68(10),* 10007-10018.

Dou, B., Whitaker, J. B., Bruening, K., Moore, D. T., Wheeler, L. M., Ryter, J., ... & van Hest, M. F. (2018). Roll-to-roll printing of perovskite solar cells. *ACS Energy Letters, 3(10)*, 2558-2565.

Gao, Z., Bumgardner, C., Song, N., Zhang, Y., Li, J., & Li, X. (2016). Cotton-textile-enabled flexible self-sustaining power packs via roll-to-roll fabrication. *Nature communications, 7(1)*, 1-12.

Jung, M., Kim, J., Koo, H., Lee, W., Subramanian, V., & Cho, G. (2014). Roll-to-roll gravure with nanomaterials for printing smart packaging. *Journal of nanoscience and nanotechnology, 14(2)*, 1303-1317.

Kim, N., Cha, S., & Peng, H. (2010). Optimal control of hybrid electric vehicles based on Pontryagin's minimum principle. *IEEE Transactions on control systems technology, 19(5)*, 1279-1287.

Kim, S. K., & Ahn, C. K. (2020). Self-tuning nonlinear control system design for roll-to-roll printing systems. *IEEE/ASME Transactions on Mechatronics, 25(6),* 2667-2676.

Lee, B., Kim, Y., Kim, J., Park, J., Kim, H., & Oh, D. (2020). Preview control of web position in roll-to-roll printing using alignment patterns. *Microsystem Technologies, 26(11)*, 3315-3321.

Lee, J., Byeon, J., & Lee, C. (2020). Theories and control technologies for web handling in the roll-to-roll manufacturing process. *International Journal of Precision Engineering and Manufacturing-Green Technology, 7(2)*, 525-544.

Lee, J., Kim, S., & Lee, C. (2019). Surface drying for brittle material coating without crack defects in large-area roll-to-roll coating system. International Journal of *Precision Engineering and Manufacturing-Green Technology, 6(4)*, 723-730.

Marchetti, L., Priami, C., & Thanh, V. H. (2017). Simulation algorithms for computational systems biology. Berlin, Germany: Springer International Publishing.

Nguyen, Q. C., Piao, M., & Hong, K. S. (2018). Multivariable adaptive control of the rewinding process of a roll-to-roll system governed by hyperbolic partial differential equations. International Journal of Control, *Automation and Systems, 16(5)*, 2177-2186.

Palavesam, N., Marin, S., Hemmetzberger, D., Landesberger, C., Bock, K., & Kutter, C. (2018). Roll-to-roll processing of film substrates for hybrid integrated flexible electronics. *Flexible and Printed Electronics, 3(1)*, 014002.

Torres, E. O. C., & Pagilla, P. R. (2018, June). Modeling and Control of Web Lateral Dynamics in Roll-to-Roll Manufacturing: New Governing Equations and Control Strategies. I*n 2018 Annual American Control Conference (ACC)* (pp. 4452-4457). IEEE.

Wang, K., Wang, H., Zhou, X., & Yang, S. (2021, July). Working Parameter Optimization of a Microstructure

Electrohydrodynamic Jet Printing System by the Quantification of Margins and Uncertainties. *In 2021 3rd International Conference on Intelligent Control, Measurement and Signal Processing and Intelligent Oil Field (ICMSP)* (pp. 134-140). IEEE.

Yoshida, T., Takagi, S., Muto, Y., & Shen, T. (2008). Modeling and resister control of sectional drive gravure printing press. *Transactions of the Japan Society of Mechanical Engineers, 74(742)*, 1438-1444.

Yoshida, T. (2008). Modeling and cooperative register control of gravure printing press. *Transactions of the Japan society of mechanical engineers C, 74(738)*, 339-345.

Zhang, T., Zheng, Y., Chen, Z., & Deng, Z. (2020). A Direct-Decoupling Closed-Loop Control Method for Roll-to-Roll Web Printing Systems. *IEEE Transactions on Automation Science and Engineering, 18(3)*, 1367-1379.

Zhou, X., Wang, D., Wang, J., & Chen, S. C. (2016). Precision design and control of a flexure-based roll-to-roll printing system. *Precision Engineering, 45*, 332-341.

Zulkowski, P. R., & DeWeese, M. R. (2015). Optimal control of overdamped systems. *Physical Review E, 92(3)*, 032117.